Volume 26
Number 15
21 April 2024
Pages 2045–2124

CrystEngComm

rsc.li/crystengcomm

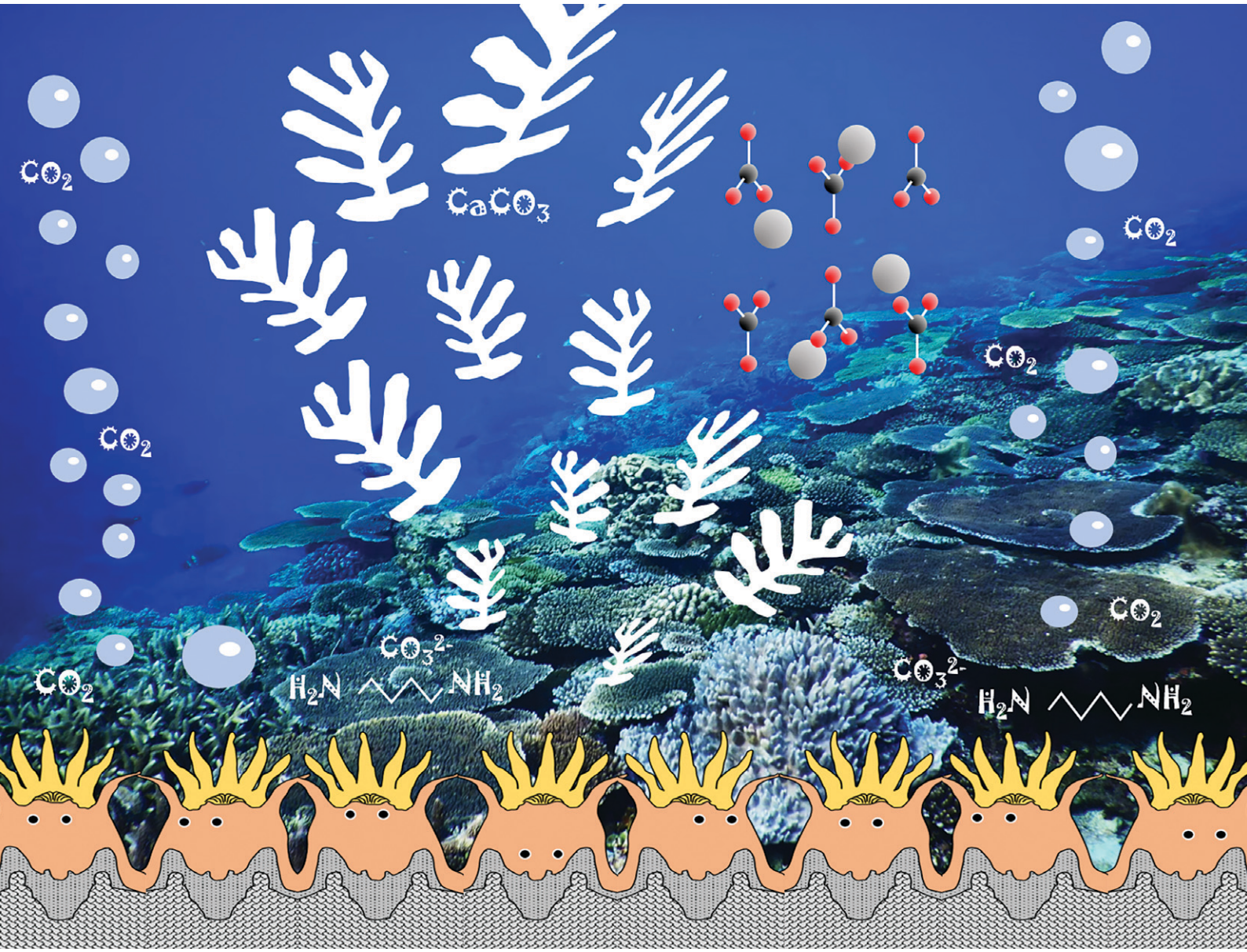

ISSN 1466-8033

ROYAL SOCIETY OF CHEMISTRY

PAPER

Hiroaki Imai *et al.*

Coral-mimetic production of aragonite films from CO_2 captured by biogenic polyamines

CrystEngComm

ROYAL SOCIETY OF CHEMISTRY

PAPER

View Article Online
View Journal | View Issue

Cite this: *CrystEngComm*, 2024, **26**, 2065

Coral-mimetic production of aragonite films from CO_2 captured by biogenic polyamines†

Kohei Takashina,[a] Hiroto Watanabe,[a] Yuya Oaki,[a] Yoshikazu Ohno,[b] Ko Yasumoto[b] and Hiroaki Imai*[a]

We designed $CaCO_3$ films comprised of aragonite nanorods by mimicking the microstructure and the formation process of the calcareous skeleton of a stony coral in the sea. Hierarchically structured calcareous frameworks are produced from the center of calcification (COC) under alkaline conditions in the organism. In the first step, a seed layer consisting of crystalline nanoparticles was produced as an artificial COC on a polyvinyl alcohol sheet in a solution containing Ca^{2+} ions, polyacrylic acid, and a biogenic polyamine, such as putrescine, through the gradual absorption of atmospheric CO_2. In the second step, aragonite nanorods grew on the artificial COC in the mother liquid obtained by mixing a putrescine solution saturated with CO_2 and a $CaCl_2$ solution containing Mg^{2+} and alginate. Finally, we obtained a dense, homogeneous film consisting of aragonite nanorods similar to the coral skeleton through the fixation of CO_2.

Received 8th February 2024,
Accepted 4th March 2024

DOI: 10.1039/d4ce00126e

rsc.li/crystengcomm

Introduction

In nature, various marine organisms fix atmospheric CO_2 as a skeleton of $CaCO_3$.[1,2] In particular, complex and huge calcareous architectures are produced by hermatypic corals. In stony coral organisms, $CaCO_3$ crystals grow in the extracellular calcifying fluid (ECF) at a high pH (Fig. S1 in the ESI†).[3,4] Recently, calcification was reported to be accelerated by the reaction of atmospheric CO_2 with biogenic polyamines having multiple amino groups (eqn (S1)–(S3) in the ESI†).[5] Thus, the formation of $CaCO_3$ is achieved by mimicking the high pH conditions similar found in the ECF in corals. The polyamine-based approach would be effective for recovering atmospheric CO_2 because thermodynamically stable $CaCO_3$ powder can be produced through low-energy processes.

Hierarchical coral skeletons exhibit calcareous structures in which aragonite fibrous crystals extend radially from a center of calcification (COC) containing organic matter (Fig. S2 in the ESI†).[6] A biogenic COC is a fibrous or sheet-like structure that is composed of low-crystalline nanoparticles of aragonite. A variety of shapes, such as those of septa and corallite walls, are controlled by the preceding formation of the COC. In an abiotic system, the construction of $CaCO_3$ structures with arbitrary shapes can be achieved by controlled crystal growth on an artificially produced COC as a seed layer. When CO_2 captured by biogenic polyamines is used as a carbonate source, immobilization of free-form structures of $CaCO_3$ has further advantages for the CO_2-recovered materials. In this study, we designed $CaCO_3$ films by mimicking the microstructure and the formation process of the calcareous skeleton of a stony coral using an artificial COC through recovery of CO_2 in association with biogenic polyamines as shown in Fig. 1.

Bioinspired calcareous hierarchical structures having nano- and micrometre-scale textures are generally produced

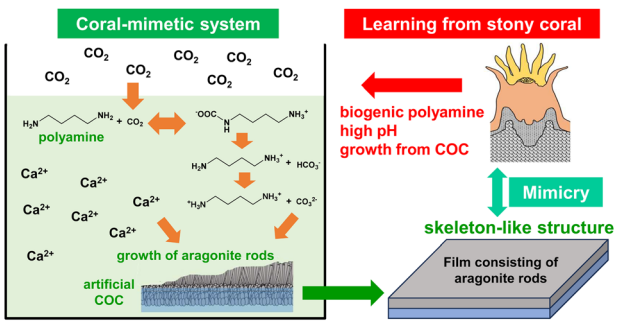

Fig. 1 Schematic illustration of the coral-mimetic production of an aragonite film. In stony corals, a $CaCO_3$ skeleton consisting of fibrous aragonite crystals is formed on the COC in the ECF under alkaline conditions. In the coral-mimetic system, a $CaCO_3$ sheet consisting of skeleton-like fibrous aragonite is produced on an artificial COC in an alkaline solution of biogenic polyamine by the capture of atmospheric CO_2.

[a] *Department of Applied Chemistry, Faculty of Science and Technology, Keio University, 3-14-1 Hiyoshi, Kohoku-ku, Yokohama 223-8522, Japan. E-mail: hiroaki@applc.keio.ac.jp*
[b] *School of Marine Biosciences, Kitazato University, 1-15-1, Kitazato, Minami-ku, Sagamihara 252-0373, Japan*

† Electronic supplementary information (ESI) available. See DOI: https://doi.org/10.1039/d4ce00126e

through crystal growth with the control of organic molecules. A wide variety of organic molecules, such as proteins,[7–9] water-soluble synthetic polymers,[10–15] and hydrogel matrices,[16–20] have been used for the production of biomimetic $CaCO_3$ mesocrystals. Specific control of the crystal phases requires the formation of metastable polymorphs, such as aragonite and vaterite. The production of various calcareous films consisting of granular domains was achieved on chitosan and polyvinyl alcohol (PVA) on a glass substrate with soluble polyanions, such as poly(acrylic acid) (PAA)[21,22] with polymorph control by the combination of insoluble and soluble organic molecules.[23,24] Basically, the presence of a particular seed layer promotes the crystal growth of the metastable phases. Prismatic vaterite films were fabricated with a silk fibroin by seeded mineralization on a polymer-coated glass substrate through a granular transition layer.[25] Aragonitic films consisting of *c*-axis-oriented nanorods were produced *via* controlled growth from a seed layer on glass and PVA substrates.[15,26] Multistep growth was developed to produce biogenic calcareous shell-like oriented nanorods of calcite using conventional polymer sheets.[18] The surface of the PVA was used as the nucleation site of calcite crystals. High-density nucleation providing the seed layer on the polymer surface is important for the formation of oriented architectures with control of the polymorph. However, coral-like structures consisting of oriented aragonite nanorods have not been achieved through recovery of CO_2 in association with biogenic polyamines. The string- and sheet-like frameworks of the COC in the coral body are biogenic seed layers for the designed construction of aragonitic architectures (Fig. S2 in the ESI†). Although polyamines were used for the structural control of $CaCO_3$,[14,15] we utilized a biogenic polyamine for the recovery of CO_2 to promote the seeded mineralization of aragonite rods. The polyamine-based approach with an artificial COC would provide a novel route for the fabrication of large hierarchical structures having nano- and micrometre-scale textures through the fixation of atmospheric CO_2.

In this work, we learned from the microstructure and calcification process of stony corals and attempted to fabricate an array of aragonite nanorods by mimicking the micro-textures of calcareous skeletons through the fixation of atmospheric CO_2 with a biogenic polyamine. First, we created a seed crystal layer consisting of aragonite nanocrystals as an artificial COC on a self-standing organic sheet. Second, we investigated the conditions for the controlled growth of oriented aragonite rods on the artificial COC from a CO_2-captured polyamine solution. The presence of Mg ions and alginate was found to be effective for the control of the polymorphs, microstructures, and homogeneity of the products. Ultimately, a suitable combination of the additives succeeded in forming an aragonite array structure similar to a coral skeleton. This fact suggests the contribution of polyamine to biomineralization, although a wide variety of functions or roles were studied for biogenic polyamines. Thus, the current study leads the bio-inspiration for the architectonics of hierarchical $CaCO_3$ structures by capturing atmospheric CO_2. Our findings would provide novel technological insight into the fabrication of highly ordered architectures by mimicking biological mineralization systems. The controlled crystal growth would be applicable to the fabrication of well-organized materials with the recovery of industrially emitted CO_2.

Results and discussion

Production of an artificial COC through selective nucleation on a self-standing polymer sheet

The biogenic COC of a coral skeleton is a fibrous or sheet-like structure that is composed of low-crystalline nanoparticles of aragonite with a large amount of organic matter. In the first step, we produced aragonite nanograins on a self-standing PVA sheet as an artificial COC (Fig. S3b in the ESI†). The smooth polymer surface covered with OH groups is suitable for the nucleation of $CaCO_3$ crystals. In aqueous solution at $[Ca^{2+}]$ = 10 mmol dm^{-3}, putrescine at 10 mmol dm^{-3}, and PAA at $[COOH_{PAA}]$ = 10 mmol dm^{-3}, the deposition of calcareous nanoparticles occurred through heterogeneous nucleation on the organic surface by the

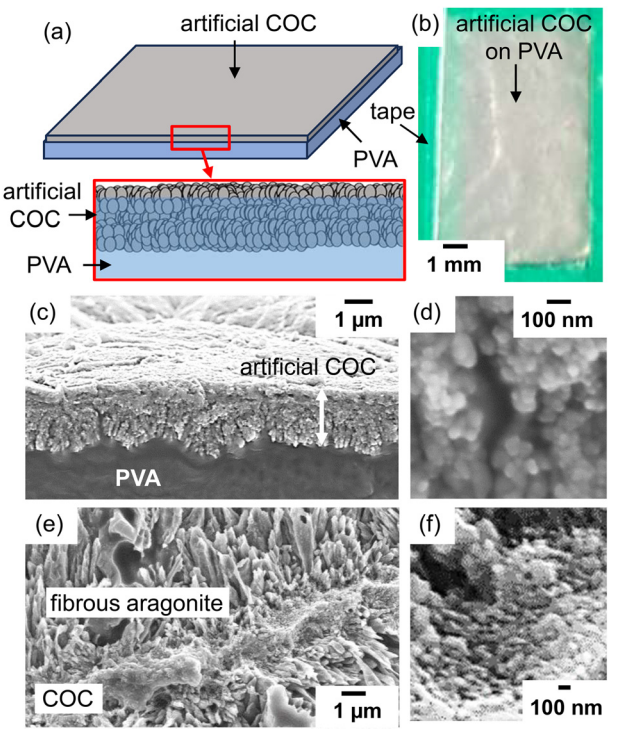

Fig. 2 A schematic illustration (a), a photograph (b), and cross-sectional SEM images (c and d) of an artificial COC layer deposited on a PVA sheet. SEM images of the biogenic COC with fibrous aragonite of a coral skeleton (*Acropora digitifera*) (e and f).[6] The green area in (b) indicates tape for fixing the PVA substrate on a glass plate. Reproduced from ref. 6 with permission from the Royal Society of Chemistry.

absorption of atmospheric CO_2 without homogeneous nucleation (Fig. 2a and b). According to SEM observation (Fig. 2c and d), a homogeneous film ~1 μm thick and consisting of nanograins ~30–80 nm in size covered the polymer sheet after being kept in air for 24 h. By mimicking the biogenic COC consisting of aragonite nanoparticles in a stony coral (Fig. 2e and f), we designed an artificial COC consisting of nanoparticles.

From Raman signals (Fig. 3a), the crystal phase of the deposition was identified as aragonite. We observed typical signals of aragonite assigned to lattice vibration modes (154 and 208 cm^{-1}) and carbonate internal modes that originate from the in-plane bending (703 cm^{-1}) of the carbonate anions.[27] The broadening of the lattice modes and a weak signal originating from carbonate ions suggest disorder of the crystal lattice. Since a weak signal attributed to the 012 diffraction of aragonite was only observed in the X-ray diffraction (XRD) pattern (Fig. 3b), the *c*-axis of low-crystalline aragonite grains was roughly arranged to be vertical to the organic substrate surface.

Calcite powder was formed through homogeneous nucleation without PAA (Fig. S4 in the ESI†). A higher ratio of PAA to Ca ions (R = $[COOH_{PAA}]/[Ca^{2+}]$) suppressed the deposition of calcite in the solution system. A suitable combination of the insoluble polymer surface and the soluble polymer resulted in the selected nucleation of aragonite. In previous reports,[28,29] the adsorption of PAA miniaturized the crystal grains and promoted the formation of mesocrystalline structures. Our results indicate that a thin film consisting of aragonite nanograins was selectively formed as a seed layer through high-density heterogeneous nucleation on the PVA surface under moderate growth conditions at R = 1.0–1.2. Since the distance between CO_3^{2-} groups of PAA on the PVA surface is similar to that on the crystal lattice of aragonite,[21] the specific nucleation is deduced to be promoted on the substrate.

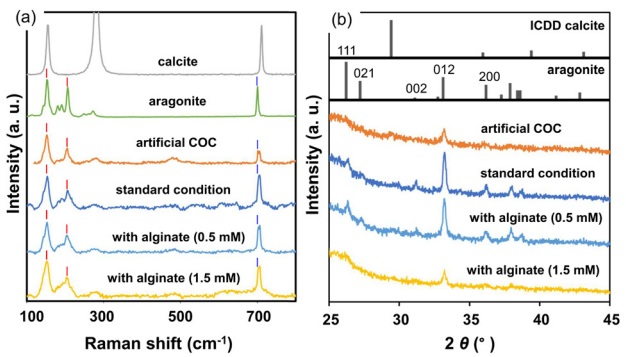

Fig. 3 Raman spectra (a) and XRD patterns (b) of the artificial COC and films produced under standard conditions with and without sodium alginate. Raman spectra of geological calcite and aragonite and ICDD patterns are shown as references. Red lines at 154 and 208 cm^{-1} and blue lines at 703 cm^{-1} in (a) indicate the lattice vibration mode of aragonite and the carbonate internal modes that originate from the in-plane bending of the carbonate anions, respectively.[27]

Formation of *c*-axis-oriented aragonite films on the artificial COC layer

For the formation of fibrous aragonite elongated along the *c*-axis on the COC layer, we replaced the growth medium with a mixture of an aqueous solution of putrescine at 30 mmol dm^{-3} that was saturated with CO_2 and a solution containing Ca and Mg ions after washing the deposited PVA film with purified water (Fig. S3c in the ESI†). The metal ion concentrations were adjusted to $[Ca^{2+}]$ = 10 mmol dm^{-3} and $[Mg^{2+}]$ = 30 mmol dm^{-3} to promote the crystal growth of fibrous aragonite on the substrate. Before the crystal growth, a CO_2-saturated putrescine solution was prepared by the bubbling of pure CO_2 (Fig. S3a in the ESI†).

As shown in Fig. 4a and b, a homogeneous layer (~4 μm thick) was produced on the artificial COC after the deposition for 3 h. Since the thickness was not changed by prolongation of the deposition, the crystal growth almost stopped within 3 h due to a decrease in the ion concentration. The crystal phase of the films was identified as aragonite from Raman spectra and XRD patterns (Fig. 3). Here, we found that fibrous aragonite grew steadily from the artificial COC layer without heterogeneous nucleation. A relatively intense 012 peak of aragonite was observed in the XRD pattern for the

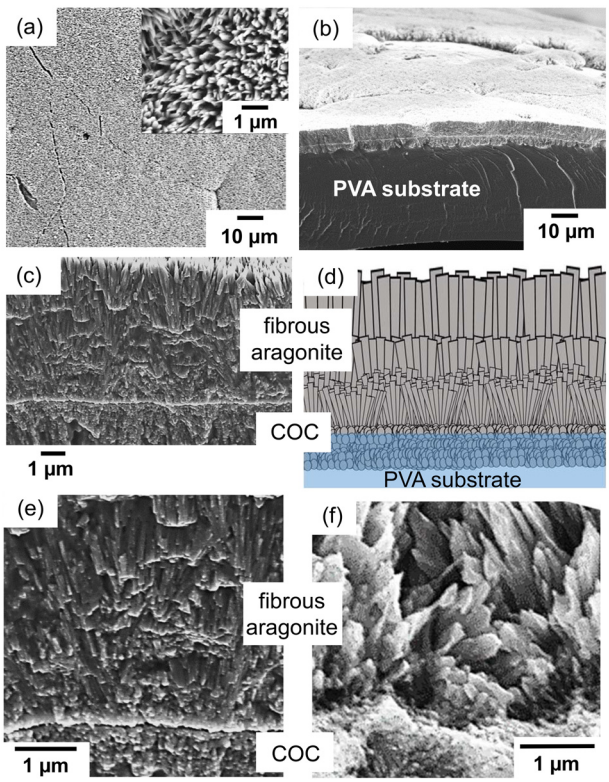

Fig. 4 SEM images (a–c and e) and a schematic illustration (d) of the film after 3 h of crystal growth in the aqueous solution containing putrescine, Ca^{2+}, and Mg^{2+}. Top (a), bird's-eye (b), and cross-sectional (c–e) views of the film. The inset of (a) is an enlarged image of the surface. SEM image of the biogenic COC of a stony coral (f).[6] Reproduced from ref. 6 with permission from the Royal Society of Chemistry.

film (Fig. 3b). Generally, aragonite is elongated in the *c* axis. As shown in Fig. S5 in the ESI,† the strong 012 peak suggests that the *c*-axis of fibrous aragonite was roughly arranged to be vertical to the substrate surface. The growth direction of all rods changed to upward in the middle of the film (Fig. 4c and d). Finally, the oriented growth of nanorods was achieved by the gradual change in growth direction in the progressive stage. We have reported the bending of $CaCO_3$ nanorods grown on a substrate.[18,26] The growth of the nanorods was gradually oriented to the direction of ion diffusion from the bulk of the solution.

In the enlarged SEM images near the bottom (Fig. 4c and e), nanorods were observed to grow from the COC layer. The growth direction of all rods changed to upward in the middle of the film with widening fibrous crystals (Fig. 4d). The width of the aragonite rods near the top was estimated to be *ca.* 200 nm. As shown in Fig. 4f, the nanoscale fibrous structure of the aragonite crystals elongated in the *c* direction is produced on the COC in the stony coral skeleton.[6] The biogenic architecture is similar to that of the synthesized layer of fibrous aragonite on the artificial COC. The cellular structures of a coral skeleton are composed of micrometric rods and sheets as shown in Fig. S2 in the ESI.† The sheet formation of aragonite rods is regarded as a basic process for the production of the cellular structures. Thus, we succeeded in demonstrating the coral-mimetic mineralization process using the artificial COC and CO_2 captured by biogenic polyamines.

When we used a solution without Mg ions, the deposition of aragonite crystals on the artificial COC layer decreased with an increase in the amount of calcite powder that was formed through homogeneous nucleation. The degree of supersaturation increased drastically by mixing the polyamine solution saturated with CO_2 and a Ca ion solution. The presence of Mg ions suppresses homogeneous nucleation and promotes the growth of the COC layer by limiting rapid crystal growth. The morphology of the aragonite rods was not affected by putrescine in our system because almost the same structures were obtained in a supersaturated solution without the molecule (Fig. S6 in the ESI†).

Formation of homogeneous films consisting of miniaturized aragonite nanorods

By addition of alginate, a soluble polysaccharide, we fabricated ordered architectures that consisted of miniaturized nanorods. In a previous study,[26] bunched nanorods 100–150 nm in diameter were formed by the addition of sodium alginate on a single-crystalline aragonite substrate (Fig. S7 in the ESI†). The miniaturization of the grown aragonite crystals was suggested to be achieved with specific interactions of alginate with the specific planes of aragonite. Fig. 5 and S6 in the ESI† show SEM images of homogeneous films consisting of aragonite nanorods that

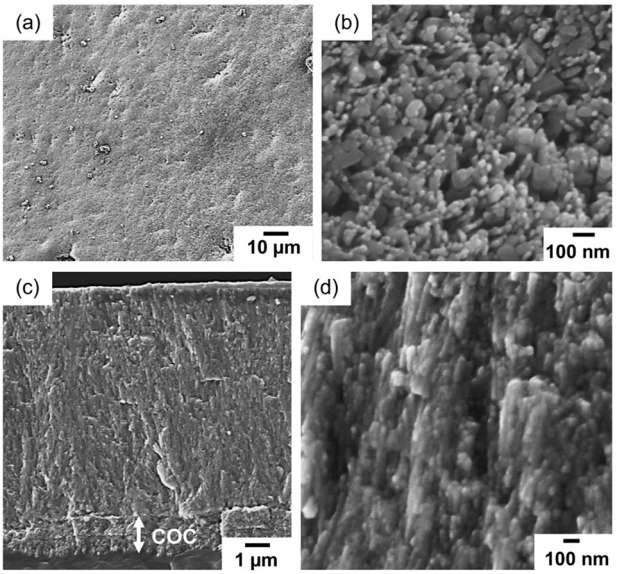

Fig. 5 SEM images (a–d) of the film after overgrowth in aqueous solution with putrescine, $[Ca^{2+}]$ = 20 mmol dm^{-3}, $[Mg^{2+}]$ = 30 mmol dm^{-3}, and $[COO^-_{alginate}]$ = 0.5 mmol dm^{-3} for 3 h. Top (a and b) and cross-sectional (c and d) views of the film.

were obtained in the solutions containing sodium alginate at $[COO^-_{alginate}]$ = 0.5 mmol dm^{-3} and $[Ca^{2+}]$ = 10 mmol dm^{-3}. A homogeneous layer ~5 μm thick was grown for 3 h in the solution mixture.

Because the intense 012 peak of aragonite was observed in the XRD pattern for the film produced with alginate (Fig. 3b), it was concluded that the aragonite nanorods were elongated in the *c* axis that was perpendicular to the substrate. The width of the aragonite rods decreased from ~200 to ~20 nm as the alginate concentration increased (Fig. 6). In our system, the crystal growth occurred in the solution phase,

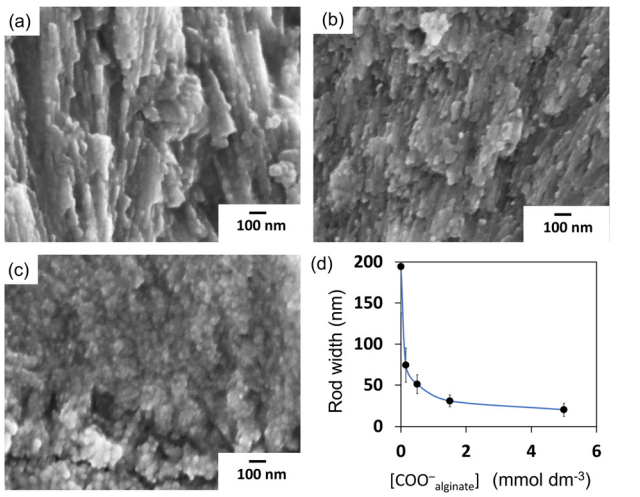

Fig. 6 Cross-sectional SEM images (a–c) and rod width as a function of alginate concentration (d) of the film after overgrowth in aqueous solution with putrescine, $[Ca^{2+}]$ = 20 mmol dm^{-3}, $[Mg^{2+}]$ = 30 mmol dm^{-3}, and $[COO^-_{alginate}]$ = 0.15 (a), 1.5 (b), and 5 mmol dm^{-3} (c).

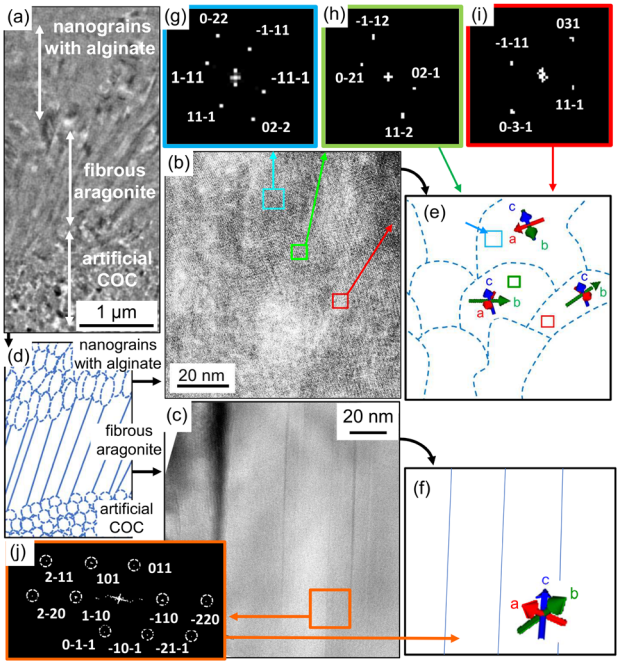

Fig. 7 TEM images (a–c) and schematic illustrations (d–f) of an FIB-cut sample of a film produced on the artificial COC under standard conditions with (b and e) and without (c and f) sodium alginate. The thin plate ~100 nm thick shows the cross-sectional structure of the film. The structural variation depending on the growth conditions is shown in (a) and (d). Colored frames (g–j) indicate the FFT patterns of the same colored areas in (b) and (c).

not in the hydrogel. The miniaturization of aragonite crystals was reported to be ascribed to the incorporation of alginate in previous work.[26] The distances between calcium ions on the (011) plane of aragonite were suggested to be relevant to the distances between carboxyl groups of alginate. Since the interaction of alginate with the specific plane partially suppresses the facet growth of the crystal, bunched thin rods are formed by branching and decreasing the length. Finally, by adjusting the concentration, we obtained a dense, homogeneous film consisting of aragonite nanorods with control of the crystal size.

Fig. 7 shows TEM images of a thin plate cut with a focused ion beam (FIB) from the film grown on the PVA surface. We observed that nanorods grew from an aggregate of nanoparticles *ca.* 10 nm, which is assigned to the artificial COC. From the fast Fourier transform (FFT) patterns, the aragonite nanorods prepared under the standard conditions were found to be elongated in the *c* direction (Fig. 7c, f and j), whereas the direction of the nanograins in the artificial COC region was random. Consequently, we obtained aragonite films that consisted of *c*-axis-oriented nanorods that were arranged perpendicularly to the surface. The upper part of the TEM image shows the thin rods produced with sodium alginate. As mentioned above, the adsorption of alginate was reported to form granular structures of calcium carbonate through deposition in aqueous systems. We observed nanograins in an enlarged TEM image (Fig. 7b). The *c* direction of the grains was roughly oriented to be perpendicular to the substrate surface according to the FFT patterns (-Fig. 7e and g–i). Here, the direction of the daughter crystals was influenced by the basal direction. Finally, weakly oriented architectures were produced on polymer sheets by the construction of granular aragonite crystals with the adsorption of the polymer molecules.

In the present study, we produced biogenic calcareous coral-like oriented nanorods of aragonite using a conventional polymer sheet. In the step for producing an artificial COC, a large number of nuclei are induced by the interaction of alcoholic hydroxy groups of the polymer surface and carboxy groups of PAA and calcium ions. The presence of alginate miniaturizes the growth units and promotes the growth of aragonite in the *c* direction. Selective growth from densely formed nuclei produces an oriented architecture consisting of aragonite rods whose *c* axis is perpendicular to the surface.

Conclusion

Coral-like calcareous films comprised of aragonite nanorods were produced by mimicking the microstructure and the formation process of the calcareous skeleton of a stony coral using atmospheric CO_2 in association with biogenic polyamines. A seed layer consisting of aragonite nanoparticles was initially fabricated as an artificial COC. Aragonite fibrous crystals were grown on the artificial COC in the mother liquid obtained by mixing a putrescine solution saturated with CO_2 and a $CaCl_2$ solution. Finally, a dense, homogeneous film consisting of aragonite nanorods was obtained through the fixation of CO_2.

Experimental

Preparation of precursor solutions

A CO_2-saturated putrescine solution was prepared as a precursor solution by bubbling CO_2 into a putrescine solution (10–30 mmol dm^{-3}) at 25 °C as shown in Fig. S3a in the ESI.† The pH value reduced to *ca.* 7 with the absorption of CO_2 and the formation of carbonate species with cationic putrescine as shown in eqn (S1)–(S3) in the ESI.† We stopped the bubbling after the pH of the solution became constant.

Production of an artificial COC through selective nucleation on a self-standing polymer sheet

We prepared fine grains of $CaCO_3$ as an artificial COC in a 60 cm^3 polypropylene vessel containing 20 cm^3 of an aqueous solution of $CaCl_2{\cdot}2H_2O$ (Junsei Chemical) containing PAA (Mw: 1800, Sigma-Aldrich). A PVA sheet (Aisero Solublon®, saponification rate >99.5%, Mw: 1700, 50 μm thick) supported on a polypropylene plate with masking tape was used as a substrate for the nucleation of $CaCO_3$ crystals. The polymer substrates were fixed vertically in the polypropylene vessel containing the precursor aqueous solution (Fig. S3b in

the ESI†). We used an aqueous solution of 10 mmol dm^{-3} $CaCl_2{\cdot}2H_2O$ (Junsei Chemical) and 10 mmol dm^{-3} putrescine containing a 10 mmol dm^{-3} carboxy group of PAA ($[COOH_{PAA}]$ = 10 mmol dm^{-3}). The solution was kept at 25 °C for 48 h with stirring for the absorption of CO_2 from the atmosphere. The resultant products were sonicated with pure water at room temperature and air dried at 25 °C for 24 h. Here, we obtained a seed layer of $CaCO_3$ as an artificial COC on the polymer sheet.

Crystal growth for *c*-axis-oriented nanorod arrays

After washing the substrate with purified water, the growth medium was changed to an aqueous solution of 10 mmol dm^{-3} $CaCl_2{\cdot}2H_2O$ and 30 mmol dm^{-3} $MgCl_2$. The CO_2-saturated putrescine solution (the precursor solution) was mixed to enhance the crystal growth for the *c*-axis-oriented nanorod arrays on the seed layer. With the suppression of homogeneous and heterogeneous nucleation, the Mg to Ca ion ratio increased to promote crystal growth from the seed. The pH of the solution decreased to 7 with the formation of $CaCO_3$. After 3 h, the exchange of the growth medium with a freshly prepared precursor aqueous solution was repeated to continue the crystal growth. We added sodium alginate (Mw: 220 000, Junsei Chemical) at various concentrations ($[COO^-]_{alginate}$ = 0.15–5 mmol dm^{-3}). The resultant products were washed with pure water and air dried at 25 °C for 24 h.

Characterization

The product structures were characterized using scanning electron microscopes (SEMs, JEOL JSM-7100F, JSM-7600F, Hitachi S-4700) and a field-emission transmission electron microscope (TEM, FEI Tecnai F20). We evaluated the crystal structure and composition of the products using X-ray diffractometry (XRD, Bruker D8 Advance), Raman scattering spectroscopy (Renishaw inVia Raman microscope), and thermogravimetry (Shimadzu DTG-60).

Author contributions

K. T., H. W., K. Y., and H. I. designed the experimental procedures and structural analysis. K. T. performed the experiments of crystal growth and characterization of the products. Y. Oaki and Y. Ohno supported the experiments and characterization. K. T. and H. I. summarized the results and reviewed the literature. H. I. supervised the project. All the authors reviewed the manuscript.

Conflicts of interest

The authors declare no competing financial interests.

Acknowledgements

This work was partially supported by JSPS KAKENHI grant number JP21H01627.

Notes and references

1 J. Feng, L. Sun and J. Yan, *Renewable Sustainable Energy Rev.*, 2023, **171**, 113018.
2 E. Tamburini, E. Turolla, M. Lanzoni, D. Moore and G. Castaldelli, *Sci. Total Environ.*, 2022, **848**, 157508.
3 Y. Ohno, A. Iguchi, C. Shinzato, M. Inoue, A. Suzuki, K. Sakai and T. Nakamura, *Sci. Rep.*, 2017, **7**, 40324.
4 D. S. Sevilgen, A. A. Venn, M. Y. Hu, E. Tambutté, D. De Beer, V. Planas-Bielsa and S. Tambutté, *Sci. Adv.*, 2019, **5**, eaau7447.
5 K. Yasumoto, M. Yasumoto-Hirose, J. Yasumoto, R. Murata, S. Sato, M. Baba, K. Mori-Yasumoto, M. Jimbo, Y. Oshima, T. Kusumi and S. Watabe, *Mar. Biotechnol.*, 2014, **16**, 465.
6 M. Sugiura, K. Yasumoto, M. Iijima, Y. Oaki and H. Imai, *CrystEngComm*, 2021, **23**, 3693.
7 S. Albeck, J. Aizenberg, L. Addadi and S. Weiner, *J. Am. Chem. Soc.*, 1993, **115**, 11691.
8 E. Weber, L. Bloch, C. Guth, A. N. Fitch, I. M. Weiss and B. Pokroy, *Chem. Mater.*, 2014, **26**, 4925.
9 J. P. R. Grajeda, A. Moreno and A. Romero, *J. Biol. Chem.*, 2004, **279**, 40876.
10 H. Cölfen and M. Antonietti, *Langmuir*, 1998, **14**, 582.
11 T. Kato, T. Suzuki, T. Amamiya, T. Irie, M. Komiyama and H. Yui, *Supramol. Sci.*, 1998, **5**, 411.
12 H. Watamura, Y. Sonobe and I. Hirasawa, *Chem. Eng. Technol.*, 2014, **37**, 1422.
13 A. N. Kulak, P. Iddon, Y. Li, S. P. Armes, H. Cölfen, O. Paris, R. M. Wilson and F. C. Meldrum, *J. Am. Chem. Soc.*, 2007, **129**, 3729.
14 A. S. Schenk, B. Cantaert, Y. Y. Kim, Y. Li, E. S. Read, M. Semsarilar, S. P. Armes and F. C. Meldrum, *Chem. Mater.*, 2014, **26**, 2703.
15 B. Wang, L. B. Mao, M. Li, Y. Chen, M. F. Liu, C. Xiao, Y. Jiang, S. Wang, S. H. Yu, X. Y. Liu and H. Cölfen, *Langmuir*, 2018, **34**, 11126.
16 S. Matsumura, S. Kajiyama, T. Nishimura and T. Kato, *Small*, 2015, **11**, 5127.
17 J. Feng, G. Wu and C. Qing, *Mater. Sci. Eng., C*, 2016, **58**, 409.
18 Y. Nagai, Y. Oaki and H. Imai, *CrystEngComm*, 2018, **20**, 1656.
19 H. Li and L. A. Estroff, *J. Am. Chem. Soc.*, 2007, **129**, 5480.
20 Y. Feng, Y.-E. Wen, X.-D. Liu, X. Xiong and Y. Jiang, *Langmuir*, 2021, **37**, 7741.
21 A. Kotachi, T. Miura and H. Imai, *Chem. Mater.*, 2004, **16**, 3191.
22 S. Kajiyama, T. Nishimura, T. Sakamoto and T. Kato, *Small*, 2014, **10**, 1634.
23 G. Falini, S. Albeck, S. Weiner and L. Addadi, *Science*, 1996, **271**, 67.
24 L. Liu, J. Jiang and S. H. Yu, *Cryst. Growth Des.*, 2014, **14**, 6048.
25 C. Xiao, M. Li, B. Wang, M. F. Liu, C. Shao, H. Pan, Y. Lu, B. B. Xu, S. Li, D. Zhan, Y. Jiang, R. Tang, X. Y. Liu and H. Cölfen, *Nat. Commun.*, 2017, **8**, 1398.

26 M. Suzuki, Y. Oaki and H. Imai, *Cryst. Growth Des.*, 2016, **16**, 3741.
27 C. G. Kontoyannis and N. V. Vagenas, *Analyst*, 2000, **125**, 251.
28 H. Cölfen and M. Antonietti, *Angew. Chem., Int. Ed.*, 2005, **44**, 5576.
29 H. Zhao, Y. Wang, Y. Yang, X. Shu, H. Yan and Q. Ran, *Appl. Surf. Sci.*, 2017, **407**, 8.